An investigation into the effect of pressure source parameters and water depth on the wake wash wave generated by moving pressure source

Mohammadreza Javanmardi[1]

Adjunct Assistant Professor, Sharif University of technology, Tehran, Iran

Jonathan Binns

Associate Dean of Research, Australian Maritime College, Launceston, Tasmania, Australia, 7250

Giles Thomas

Professor, University College London, Torrington Place, London WC1E 7JE, UK

Martin Renilson

Adjunct Professor, University of Tasmania, Launceston, Tasmania, Australia, 7250

Abstract

In this study the effect of moving pressure source and channel parameters on the generated waves in a channel was numerically investigated. Draught, angle of attack and profile shape were investigated as parameters of pressure source and water depth and blockage factor as channel parameters on wave height. Firstly, the chosen Computational Fluid Dynamics (CFD) approach was validated with the experimental data over a range of speed. Then the CFD study was conducted for further investigations. It was shown that that by enlarging draught, angle of attack and beam of the pressure source, the wave height generated will be increased. Channel study showed that it is possible to increase the wave height generated by shallowing water for a given speed as long as the depth Froude number is subcritical and the wave height generated is independent of water depth for supercritical depth Froude numbers. The blockage factor has more influence at supercritical Froude depth values, while at subcritical Froude values is negligible compare with water depth.

Keywords

Wake wash, wave propagation, Computational Fluid dynamics, Towing Tank, Pressure Source

Introduction

The wake pattern which is produced by a moving point across the surface of deep water was first explained mathematically by Lord Kelvin (William Thomson) [1] and is known as the Kelvin wake pattern. All vessels operating in deep water produce a Kelvin type wave pattern consisting of two

[1] Corresponding author
Email: mj00@utas.edu.au
Fax: +982166165563
Present address: Marine Lab., Sharif University of Technology, Tehran, Iran

kinds of waves: transverse waves which crest across the ship track and divergent waves which crests roughly parallel to the ship track, moving outward. The waves are confined to a wedge shaped region behind the ship, and the half angle of the wedge is 19.5 degrees. This angle is independent of the ship speed as long as the deep water condition is satisfied.

Many studies have been conducted into the effect of waves on vessels operating in shallow and restricted waterways, for example [2, 3]. In addition, significant research has been conducted into wash wave impacts on ecology and the environment, and vessel operation in shallow water close to the coastline [4].

The wash waves generated by vessels can be also characterized in terms of the hull shape [5] and operating condition [6]. Due to the great interest in wake wash effects, a considerable amount of research effort has been conducted in recent years. In model experimental studies the focus has been on designing low-wash ships and acquiring reliable data for validation [7-9].

Most research has been conducted using theoretical [10] or experimental [11, 12] approaches. For a ship moving in water of uniform depth, linear and nonlinear theories can be applied usefully in the subcritical and the supercritical speed range [13, 14]. Thin ship theory can be used for the wave generation by a ship moving in a channel. This theory provides an alternative to higher order panel methods for estimating wave resistance when applied solely to slender hulls [10], but it is not valid for unsteady cases and transom stern flow separation [13]. More general shallow-water approximations are obtained from Boussinesq type equations, which are valid for most arbitrarily unsteady cases. Boussinesq's equations based on a suitable reference level were used for computing ship waves in shallow water. However this method is not able to predict the 3D flow pattern around the vessel [15]. An alternative is to combine the thin ship theory and the Boussinesq method. This hybrid approach combines a steady nonlinear panel method for the near-ship flow with a Boussinesq solver for the far-field wave propagation [13]. However, this method is only useful for steady problems. It should be noted that due to the nonlinear and unsteady nature, as well as the large domain feature of the wash problems, they can be neither solved well by the linear wave theory nor approximated efficiently by nonlinear singularity methods. Typically, the finite volume method has been used to predict the wave generated and its propagation [15, 16]. Previous studies by the authors showed that the numerical approach can predict wave propagation accurately [17, 18].

In the present study, a pressure source model was tested at Australian Maritime College Towing Tank at different speed and the generated waves parameters were captured by wave probes. Next, the simulations were conducted by ANSYS-Fluent software version 14.5 in same condition as the experimental. Through the comparison of computed and measured results, applicability of the numerical method is examined. Subsequently the numerical approach was used for further investigation.

Experimental setup

In order to generate waves, a moving wavedozer model was used as a pressure source during the experimental. The wavedozer model [19] is a wedge shape model with the constant beam (Figure). The main particulars of the wavedozer are listed in Table .

This model was tested at the Australian Maritime College towing tank which has a length of 100m, and a width of 3.5m. The water depth for the tests was 1.5m in all conducted tests. Three wave probes were positioned at 0.75, 1.0 and 1.25 m from the centre-line of the model to record the wave parameters (Figure), where y^* is defined by the distance of the wave probe position over the width of the channel ($y^*=y/W$). Two load cells were installed on the model to measure the vertical and drag forces. The model was tested at various depth Froude numbers from 0.43 to 0.99.

Numerical simulation

The CFD software ANSYS-Fluent version 14.5 was used as the flow solver [20]. The governing equations are three-dimensional Reynolds Averaged Navier-Stokes equations for incompressible flows. The Volume of Fluid (VOF) approach was used with a time-dependent and explicit time discretization scheme employed to solve the equations. The SIMPLE algorithm was used for the pressure-velocity coupling and the PRESTO scheme for the pressure interpolation. The k-epsilon model with the standard wall function was utilized for turbulence modelling. The 2nd order upwind scheme was used for solving the momentum equations and the High Resolution Interface Capturing scheme (HRIC) for the solution of the volume fraction equations.

Figure 34 shows the computational grid domain. For the numerical investigation, a domain comprising 6m in front of the model and 13.5m behind it was considered. The heave and trim were fixed at the same value as used in experimental tests. As the flow has a plane of symmetry about the centre plane, to decrease the processing time, half of the domain was used. The origin of the coordinate system was located at the middle of the model. The open channel boundary condition was used to specify the inlet and outlet boundary condition. Inlet velocity and outflow boundary conditions were selected for inlet and outlet boundaries respectively. A symmetry plane was used along the centre plane, and the remaining boundary surfaces along the exterior of the domain were set to no-slip wall conditions. The more details about mesh domain and cells’ properties are presented in (21).

Validating the numerical approach

The results of the numerical simulation have been compared with experimental data in various figures. Figure shows the drag coefficient results for the experimental and numerical investigations, and Figure presents the vertical force (or lift) coefficient for different speeds. Drag and vertical force coefficients are defined as:

$$C_d = \frac{Drag}{0.5 \times \rho \times V^2 \times D \times B} \tag{1}$$

$$C_l = \frac{Vertical\ Force}{0.5 \times \rho \times V^2 \times LWL \times B}$$

Where ρ is water density, V is speed of the pressure source, D is draught, B is beam and LWL is length of waterline. It should be mentioned, the water separates from model sides during tests and only model bottom remains wet (21). In addition, the highest portion of total drag (95%) can be attributed to pressure drag (21). Therefore, in Equation 1, the area is equal $D \times B$ and in Equation 2, the area is equal $LWL \times B$. The standard error bars (5%) were shown for all the experimental data.

It is clear that the simulation results are in good agreement with the experimental data with respect to the forces. The percentage variations between numerical results and the experimental data are mostly less than 5%. To increase the accuracy of the results for lower speed, the mesh should be refined, however in this study the higher speeds are more interested. The free-surface elevation for depth Froude numbers 0.7 and 0.99 for nearest, middle and farthest wave probes are presented in Figure to Figure . Free-surface elevations show the Fluent software is able to predict the wave patterns at different lateral distances. According to presented results, the numerical method is validated, and can be used to investigate the effects of changes in parameters. It should be mentioned that first wave behind the pressure source was considered as surfable wave, therefore surface elevation of the first wave behind the pressure source was considered and as soon as the first wave reached to steady state, the simulations were stopped. To improve the accuracy of the results in far filed the simulation time should be increased and mesh should be refined, however in this study was unnecessary.

Investigating the effect of various parameters

Pressure source parameters

Draught, beam and angle of attack are the main parameters of the wavedozer which were numerically investigated with respect to the wave generated height and propagation. Changing any of these parameters will alter the wavedozer's displacement. In this study, only one of the parameters was changed at a time and the rest kept constant in order to compare the numerical results and examine the effect of the changed parameter.

Draught

	Draught (m)	Beam (m)	Angle of attack (deg)	LWL (m)	Displacement (m^3)	Blockage factor
Model 1	0.1	0.3	14	0.40	0.006015	0.0057
Model 2	0.12	0.3	14	0.48	0.00866	0.0068

Table shows the dimensions of two wavedozers. Model 1 is the model which was used in the experimental tests and the previous simulations. To consider the effect of draught on generated waves, a new model (Model 2) was simulated. The draught of Model 2 was 20% more than Model 1. These simulations were conducted in deep water condition (1.5 m water depth). Since the tests were conducted in 1.5 m water depth, the draught change does not have a significant influence on the blockage factor. Blockage factor can be defined as:

$$Blockage\ factor\ (\kappa) = \frac{Model\ cross\ section\ area\ (A_S)}{Channel\ cross\ section\ area\ (A_C)} \quad (3)$$

The comparison between Model 1 and Model 2 shows that increasing the draught causes an increase in wave height. It is predicted there is a specific draught which generated wave starts to break and increasing draught more, does not have effect on the generated wave height. Figure to Figure present the wave heights comparison for two different models at different lateral distances, where y is lateral distance, B and W are model and channel widths respectively, *H* is wave height of first wave behind the pressure source and *h* is water depth.

Angle of attack

Another potentially important parameter is the angle of attack. The angle of attack is the angle between the entry surface and the water surface. The previous studies were conducted with a wavedozer with a 14 degree angle of attack. The 14 degree angle of attack was presented as the optimum angle in [19]. In this study, wavedozers with different angles of attack were simulated. By altering the angle of attack, the length of water line (LWL) and the displacement will be changed and the draught and beam remained constant. The wavedozer with the lowest angle of attack has the largest displacement and vice versa.

	Draught (m)	**Beam (m)**	**Angle of attack (deg.)**	**LWL (m)**	**Displacement (m^3)**	**Blockage factor**
Model 1	0.1	0.3	14	0.401	0.006015	0.0057
Model 3	0.1	0.3	10	0.567	0.008505	0.0057
Model 4	0.1	0.3	7	0.814	0.01221	0.0057
Model 5	0.1	0.3	4	1.43	0.02145	0.0057

Table presents the wavedozers parameters. Figure to Figure illustrate the wave heights for different wavedozers at different Fr_h.

By decreasing the angle of attack, the variation of wave height with lateral distances decreases. For example, for Model 5 (angle of attack of 4 degree) at $Fr_h = 0.9$, the wave height is almost constant for the entire width of the channel. By increasing the angle of attack, the maximum wave height is increased due to increasing the pressure gradient. It can be said that $\frac{D}{LWL} \alpha \frac{\delta p}{\delta x}$, where $\frac{\delta p}{\delta x}$ is pressure gradient in longitudinal direction (p is pressure force). Therefore by increasing the angle of attack for constant draught (D) the length of waterline (LWL) will decrease. Therefore, the pressure gradient will increase, and as a consequence, the wave generated height will increase. Model 5 has the largest displacement while it generates the lowest wave height. Increasing the displacement by changing the angle of attack (or LWL) has the opposite effect on wave height. By decreasing the angle of attack the model drag decreases. Figure and Figure show the drag and vertical forces for different angle of attack. The highest portion of total drag can be attributed to pressure drag (21). Increasing the angle of attack increases the pressure drag and decreasing the angle of attack increases the wetted area and as a result increases the viscous drag. It can be concluded that Model 5 with the largest displacement generates the lowest wave height because it has minimum pressure drag, and Model 1 with lowest displacement generated the highest wave height because it has maximum drag.

Beam

The effect of pressure source beam on the generated wave height and quality was investigated. For this investigation, the wavedozer beam was increased from 300mm (model 1) to 433mm (model 6). In addition, it should be noted that the wavedozer with 433mm beam (Model 6) has the same displacement as the model with 120mm draught (model 2) which was used previously for the draught investigation.

	Draught (m)	Beam (m)	LWL (m)	Water plane (m^2)	Angle of attack (degree)	Volume displacement (m^3)
Model 1	0.1	0.3	0.40	0.120	14	0.006
Model 2	0.12	0.3	0.48	0.144	14	0.00866
Model 6	0.1	0.433	0.40	0.174	14	0.00866

Table presents the characteristics of these models. Therefore, by comparing models 1 and 6, it is possible to see the effect of beam and displacement change on wave height and by comparing models 2 and 6, make it possible to see the effect of altering beam and draught, but maintaining displacement. The simulations were conducted in a channel with 3.5m width and 1.5m depth. Figure to Figure illustrate the results for the aforementioned models at different Fr_h.

The results show that by increasing the model beam, the generated wave height increases for all investigated Fr_h. The wave height of model 6 which has greater beam (the width of model 6 is about 44% larger than models 1 and 2) is about 28% to 98% larger than wave height for models 1 and 2 at various lateral distances. The comparison between models 1, 2 and 6 shows that adding displacement increases wave height, however the increase by increasing draught is small, whereas the increase due to a beam increase is large. The difference between models 6 and 2 can be explained by considering that the waterplane of Model 6 is larger than Model 2 (

	Draught (m)	Beam (m)	LWL (m)	Water plane (m^2)	Angle of attack (degree)	Volume displacement (m^3)
Model 1	0.1	0.3	0.40	0.120	14	0.006
Model 2	0.12	0.3	0.48	0.144	14	0.00866
Model 6	0.1	0.433	0.40	0.174	14	0.00866

Table). Therefore increasing the displacement by increasing the beam generates a higher wave than increasing the draught. It is predicted that increasing the beam will increase the wave height till wave starts to break and then further increase of beam does not have influence on the wave height.

Pressure source profile shape

According to the angle of attack study results, it was seen that the waves generated by a 4 degree angle of attack model had almost constant height across the channel while the model with angle of attack of 14 degrees generated higher waves. However, the bow waves generated by the 4 degree angle of attack were larger than those of the 14 degree angle of attack. A new model (model 8) was generated. This model has a constant beam, with a 14 degree angle of attack at the front and a 4 degree angle of attack at the stern (

Beam (m)	0.3
Length of water line (m)	0.4
Angle of attack in front (degree)	14
Angle of attack in stern (degree)	4
Draught (m)	0.1

Table). Figure shows model 8 schematically. Figure to Figure show the results between model 1 (14 degree angle of attack), model 5 (4 degree angle of attack) and model 8. The wave generated heights for model 8 are smaller than those of model 1, but the wave height decrease of between y^*=0.57 and y^*=0.71 lateral distances is slightly less compared to model 1.

According to the results, it can be concluded that the angle of attack in front of model (at the stagnation point) is more effective in wave generated height. While the angle of attack at transom can has effect on wave quality. It means, the wave height decrease of between 1.0 m and 1.25 m lateral distances is slightly less compared to model 1 and more than model 8.

Channel parameters

Depth

The effect of water depth on generated wave height was investigated. Three water depths were considered and the wavedozer with 0.1 m draught and 0.3 m beam was simulated at three different speeds. The only difference between channels was the water depth.

	V [m/s] / ***h* [m]**	**1.66**	**1.99**	**2.66**
Channel 1	0.4	0.838	1	1.343
Channel 2	0.45	0.79	0.947	1.266
Channel 3	0.5	0.75	0.9	1.2

Table presents Fr_h for the given speeds at different water depths. Fr_h values at 1.66 m/s forward speed for all three different depths are less than 1 (sub-critical Fr_h) . Figure shows the wave height results at 1.66 m/s speed for the three different water depths. According to the results, the generated wave in the shallowest water has the largest wave height, because it has the highest Fr_h.

The Fr_h at 1.99 m/s speed and 0.4 m water depth is equal to 1. The simulation results show the generated bow wave (soliton wave) at this condition is larger than for the two other conditions and the wave behind the pressure source has the lowest height at Fr_h=1.0 (Figure). Figure presents the wave heights at diffirent lateral distances for three different water depths at 1.99 m/s speed. Figure presents the results for 2.66 m/s at different water depths. The Fr_h for all three conditions are larger than 1. Figure shows the time history of surface elevation at 0.75 lateral distances for 2.6 m/s speed at three different water depths. It can be seen that the shape of the waves are the same for Fr_h larger than 1.2. It means the water depth does not have influence on the wave shape. Because the Fr_h values are greater than one, the downstream pressure does not have an effect on the up-stream.

Blockage factor

By changing the water depth, depth Froude number and blockage factor will change simultaneously. It was shown in the previous section that changing the water depth has an effect on the generated wave characteristics. To separate the effect of depth Froude number and blockage factor by changing the water depth, a new channel was modelled (channel 4) and the results were compared with the two other channels results.

	Width (m)	**Depth (m)**	**Blockage factor (κ)**
Channel 1	3.5	0.4	0.0214
Channel 3	3.5	0.5	0.0171
Channel 4	4.375	0.4	0.0171

Table presents the parameters of the three channels which were used for this comparison. Channels 1 and 4 have the same water depth, and channels 3 and 4 have the same blockage factor but different water depths. The results for the three different speeds 1.66, 1.99 and 2.66 m/s are presented in Figure to Figure .

The results indicate that the effect of depth Froude number on wave height is more important than the blockage factor for Fr_h<1.0 and the blockage factor at this range of Fr_h is negligible. Therefore, higher Fr_h generates larger wave (Figure 34). In Figure 35, model in Channel 3 is in sub-critical (Fr_h=0.9) and model in Channels 1 and 4 are in critical (Fr_h=1.0) Froude depth values. At supercritical Froude depth values the channel with lowest blockage factor generates the highest wave (Figure 36). More investigations are required to find the highest ineffective blockage factor. At highest ineffective blockage factor the channel cross section would be smallest cross section which does not have influence on the wave generated parameters.

Concluding remarks

In this study the influence of pressure source parameters, depth and blockage factors were investigated. Draught, angle of attack, beam and profile shape were investigated as the effective parameters of pressure source on wave height. Since the first wave behind the pressure source was considered as surfable wave, the effect of parameters on this wave was investigated.

The investigation indicated that increasing draught, angle of attack and beam will increase the wave height generated, while it was shown that wave height variation across the channel for a lower angle of attack is less than others. The pressure gradient will increase by increasing the angle of attack. Hence the wave generated by higher angle of attack wavedozer is larger than the lower. Comparing the results for the two different wavedozers with the same displacement and angle of attack, but different beam and draught, it can be seen that the model with the wider beam generates a higher wave. This means that the effect of beam on generated waves is greater than the effect of draught. The model with larger beam has larger water plane which means the volume of displacement close to free surface for model with larger beam is bigger than the model with larger draught. Consequently, the wave generated by wider wavedozer is higher than other one. Meanwhile, it is expected that there is limitation for effective draught and the draught larger than that does not have effect on wave generated height. Since only the portion of displacement close to free surface has effect on the wave generated. Increasing the beam with increase the wave height till the wave generated does not break.

The water depth study showed that by decreasing the water depth for a given speed, larger wave height will be generated as long as the Fr_h is subcritical. When Fr_h=1 the bow (soliton) wave generated is higher than the wave behind the pressure source. It was also shown that water depth does not have an effect on the wave height for Fr_h more than 1.2. It means for this range of Fr_h the downstream does not have influence on upstream, because the pressure source moves faster than wave speed.

The blockage factor was investigated. The results indicate that the effect of depth Froude number on wave height is more important than the blockage factor for subcritical Froude depth values and the blockage factor at this range is negligible. At supercritical Froude depth values the channel with lowest blockage factor generates the highest wave. Further simulations are needed to find the highest ineffective blockage factor.

Acknowledgement

The authors thank the Australian Research Council (ARC), University of Tasmania, and Liquid Time Pty Ltd., which funded this research. This research was supported under the ARC Linkage Projects funding scheme (Project LP0990307).

References

[1] Georgiadis, C. “Modeling Boat Wake Loading on Long Floating Structures,” *Computers & Structures*, vol. 18, no. 4, pp. 6 (1984).

[2] Dam, K. T., Tanimoto, K., Nguyen, B. T. and Akagawa, Y. “Numerical Study of Propagation of Ship Waves on a Sloping Coast,” *Ocean Engineering*, vol. 33, pp. 15 (2006).

[3] Jiankang, W., Lee, T. S. and Shu, C. “Numerical Study of Wave Interaction Generated by Two Ships Moving Parallely in Shallow Water,” *Computer Methods in Applied Mechanics and Engineering*, vol. 190, pp. 12 (2001).

[4] Nanson, G., Krusenstierna, A. V., Bryant, E. and Renilson, M. “Experimental Measurements of River Bank Erosion Caused by Boat-Generated Waves on the Gordon River, Tasmania,” *Regulated Rivers, Research and Management*, vol. 9, pp. 14 (1994).

[5] Renilson, M. R. and Lenz, S. "An Investigation into the Effect of Hull Form on the Wake Wave Generated by Low Speed Vessels.", *22nd American Towing Tank Conference*, p. 6 (1989).

[6] Robbins, A., Thomas, G., Renilson, M. and Macfarlane, G. “Subcritical Wave Wake Unsteadiness,” *RINA Transactions, International Journal of Maritime Engineering*, vol. 153, Part A3 (2011).

[7] Zibell, H. G., and Grollius, W. "Fast vessels on inland waterways.", in *The RINA International Conference on Coastal Ships and Inland Waterways*, London, England (1999).

[8] Macfarlane, G. J. and Bose, N. “Wave Wake: Focus On Vessel Operations Within Sheltered Aterways,” *SNAME*, vol. 006 (2012).

[9] Koushan, K., Werenskiold, P. and Zhao, R. “Experimental And Theoretical Investigation Of Wake Wash,” in *FAST*, Southampton, UK, pp. 165-179 (2001).

[10] Chandraprabha, S. and Molland, A. F. “A Numerical Preiction Of Wash Wave And Wave Resistance Of High Speed Displacement Ships In Deep And Shallow Water,” in *Conference Of Mechanical Engineering Network Of Thailand*, Khon Kaen, Thailand (2004).

[11] Fontaine, E. and Tulin, M. P. “On The Prediction Of Nonlinear Free-Surface Flows Past Slender Hulls Using 2D+T Theory: The Evolution Of An Idea,” in *Fluid Dynamics Of Vehicles Operating Near Or In The Air-Sea Interface*, Amsterdam, Netherland (1998).

[12] Henn, R., Sharma, S. D. and Jiang, T. “Influence Of Canal Topography On Ship Waves In Shallow Water,” in *16th International Workshop On Water Waves And Floating Bodies*, Hiroshima, Japan (2001).

[13] Yang, Q., Faltinsen, O. M. and Zhao, R. “Wash Of Ships In Finite Water Depth,” in *FAST*, Southhampton, UK, pp. 181-196 (2001).

[14] Raven, H. C. “Numerical Wash Prediction Using A Free-Surface Panel Code,” in *International Conference on Hydrodynamics of High-Speed Craft - Wake Wash and Motion Control*, London, UK (2000).

[15] Kofoed-Hansen, H., Jensen, T. and Sørensen, O. R. “Wake Wash Risk Assessment Of High-Speed Ferry Routes – A Case Study And Suggestions For Model Improvements,” in *International Conference on Hydrodynamics of High-Speed Craft - Wake Wash and Motion Control*, London, UK (2000).

[16] Kim, Y. “Artificial Damping In Water Wave Problems II: Application to Wave Absorption,” *International Journal of Offshore and Polar Engineering*, vol. 13, pp. 5 (2003).

[17] Javanmardi, M., Binns, J., Renilson, M. R., Thomas, G. and Huijsmans, R. “The Formation Of Surfable Waves In A Circular Wave Pool- Comparison Of Numerical And Experimental Approaches,” in *31th International Conference on Ocean, Offshore and Arctic Engineering*, Rio de Janeiro, Brazil (2012).

[18] Javanmardi, M., Binns, J., Thomas, G. and Renilson, M. R. "Prediction Of Water Wave Propagation Using Computational Fluid Dynamics." in *32th International Conference on Ocean, Offshore and Arctic Engineering*, Nantes, France (2013).

[19] Driscoll, A., and Renilson, M. R. “The wavedozer. A system of generating stationary waves in a circulating water channel,” *AMTE(H) TM80013* (1980).

[20] "ANSYS FLUENT User's Guid," ANSYS, Inc. (2011).

Mohammadreza Javanmardi is Adjunct Assistant Professor at Sharif University of Technology. His research focusses on the ship hydrodynamics, maneuvering, wave, Computational Fluid Dynamics and experimental tests.

A/ Professor Jonathan Richard Binns, Associate Dean Research, Australian Maritime College; Director, ARC Research Training Centre for Naval Design and Manufacturing, University of Tasmania. Jonathan Binns has trained and worked as a design and research engineer specialising in analysis of fluid mechanics by theoretical and experimental means. His primary expertise is in a variety of model and full scale experiments as well as potential flow and finite volume flow predictions. Jonathan has experience in hydrodynamic and structural design, research, development and simulation of marine craft.

Martin Renilson is an Adjunct Professor in Hydrodynamics at the University of Tasmania. His previous experience includes as Technical Manager and Deputy General Manager for the Maritime Platforms and Equipment Group at QinetiQ.

Giles Thomas is BMT Chair of Maritime Engineering in University College London's Department of Mechanical Engineering. A naval architect, his research focusses on the performance of ships, boats and offshore structures. Specific interests include fluid-structure interaction, hydrodynamics, full scale measurements, model testing and design. He is a Fellow of the Royal Institution of Naval Architects (RINA) and a Chartered Engineer (CEng – Engineering Council of Great Britain).

Figure captions

Figure 1. Wavedozer model attached to the towing Tank carriage.

Figure 2. Layout of probes with pressure source.

Figure 3. Computational grid domain.

Figure 4. Comparison of experiment and numerical drag coefficients for different Fr_h at 1500mm water depth.

Figure 5. Comparison of experiment and numerical lift coefficients for different Fr_h at 1500mm water depth.

Figure 6. Free-surface elevation for Fr_h=0.7 at 750mm lateral distance from centre-line (WP1).

Figure 7. Free-surface elevation for Fr_h=0.99 at 750mm lateral distance from centre-line (WP1).

Figure 7. Free-surface elevation for Fr_h=0.99 at 1000mm lateral distance from centre-line (WP2).

Figure 8. Free-surface elevation for Fr_h=0.99 at 1250mm lateral distance from centre-line (WP3).

Figure 9. Non-dimensional wave heights variation with respect to lateral distances for model 1 and model 2 at Fr_h=0.75.

Figure 10. Non-dimensional wave heights variation with respect to lateral distances for model 1 and model 2 at Fr_h=0.9.

Figure 12. Non-dimensional wave heights variation with respect to lateral distances for model 1 and model 2 at Fr_h =0.95.

Figure 13. Non-dimensional wave heights variation with respect to lateral distances for model 1 and model 2 at Fr_h =0.99.

Figure 11. Wave height generated variation with respect to angle of attack (AoA) at different lateral distances for Fr_h=0.75.

Figure 12. Wave height generated variation with respect to angle of attack (AoA) at different lateral distances for Fr_h=0.9.

Figure 13. Wave height generated variation with respect to angle of attack (AoA) at different lateral distances for Fr_h=0.95.

Figure 14. Wave height generated variation with respect to angle of attack (AoA) at different lateral distances for Fr_h=0.99.

Figure 15. The drag coefficients variation with respect to Angle of Attack at different Fr_h.

Figure 16. The lift coefficients variation with respect to Angle of Attack at different Fr_h.

Figure 17. Non-dimensional wave heights variation with respect to lateral distances for models 1, 2 and 6 at Fr_h=0.75.

Figure 18. Non-dimensional wave heights variation with respect to lateral distances for models 1, 2 and 6at Fr_h=0.9.

Figure 19. Non-dimensional wave heights variation with respect to lateral distances for models 1, 2 and 6at Fr_h=0.95.

Figure 20. Non-dimensional wave heights variation with respect to lateral distances for models 1, 2 and 6 at Fr_h=0.99.

Figure 21. Model 8 of B=0.3m, LWL=0.4m, AOA at transom=4 degrees, AOA at front=14 degrees and D=0.1m.

Figure 22. Non-dimensional wave heights variation with respect to lateral distances for model 1, 5 and 8 for Fr_h=0.75.

Figure 23. Non-dimensional wave heights variation with respect to lateral distances for model 1, 5 and 8 for Fr_h=0.9.

Figure 24. Non-dimensional wave heights variation with respect to lateral distances for model 1, 5 and 8 for Fr_h=0.95.

Figure 25. Non-dimensional wave heights variation with respect to lateral distances for model 1, 5 and 8 for Fr_h=0.99.

Figure 26. Non-dimensional wave heights variation with respect to lateral distances for three different water depths at 1.66 m/s speed.

Figure 27. Free-surface elevation at 0.75 m lateral distances at 1.99 m/s speed for three different water depths.

Figure 28. Non-dimensional wave heights variation with respect to lateral distances for three different water depths at 1.99 m/s speed.

Figure 29. Non-dimensional wave heights variation with respect to lateral distances for three different water depths at 2.66 m/s speed.

Figure 30. Free-surface elevation at 0.75 m lateral distances at 2.66 m/s speed for three different water depths.

Figure 31. Wave heights variation with respect to lateral distances for three different water depths at 1.66 m/s speed.

Figure 32. Wave heights variation with respect to lateral distances for three different water depths at 1.99 m/s speed.

Figure 33. Wave heights variation with respect to lateral distances for three different water depths at 2.66 m/s speed.

Table captions

Table 1. Wavedozer Principal Particulars.

Table 2. Wavedozers dimensions.

Table 3. Wavedozers with different angle of attack parameters.

Table 4. The pressure sources characteristics.

Table 5. The characteristics of model 8.

Table 6. Fr_h for different speeds at different water depth.

Table 7. Three different channels parameters for blockage factor investigation.

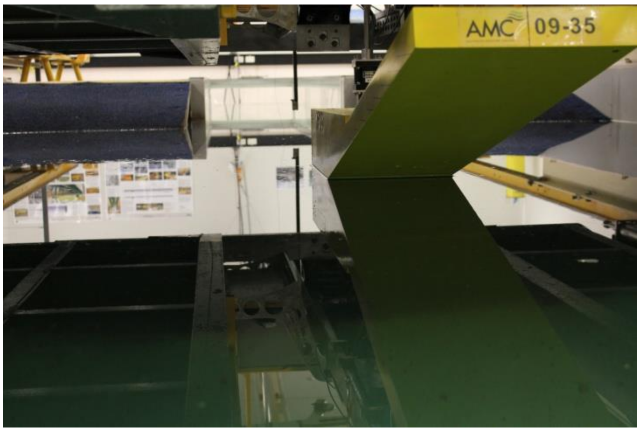

Figure 1.

Length (m)	1.5
Beam (m)	0.3
Draft(m)	0.1
Angle of attack (deg.)	14

Table 1.

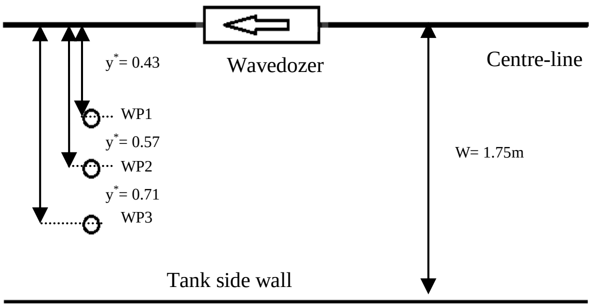

Figure 2.

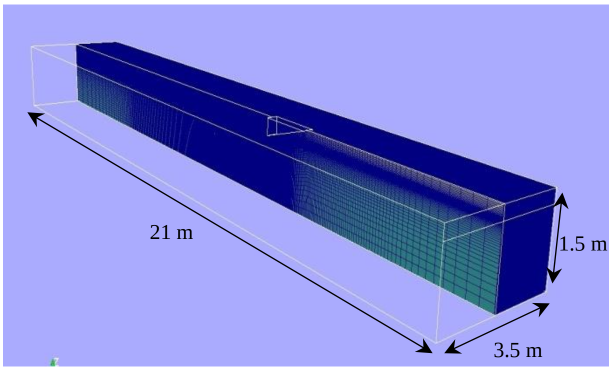

Figure 34.

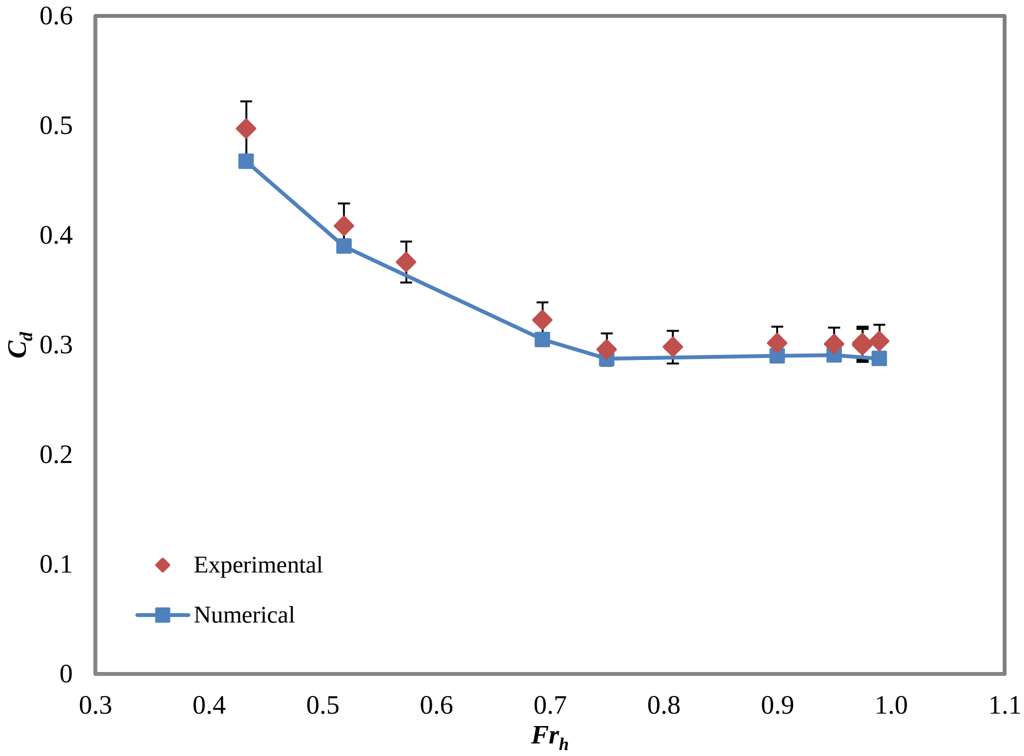

Figure 4.

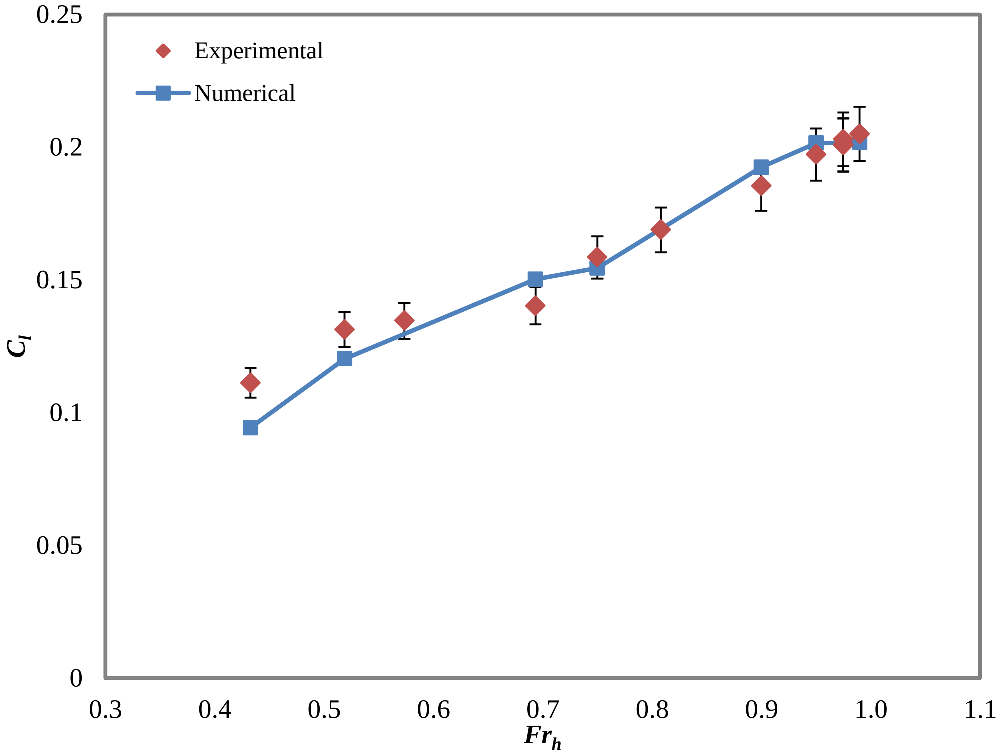

Figure 5.

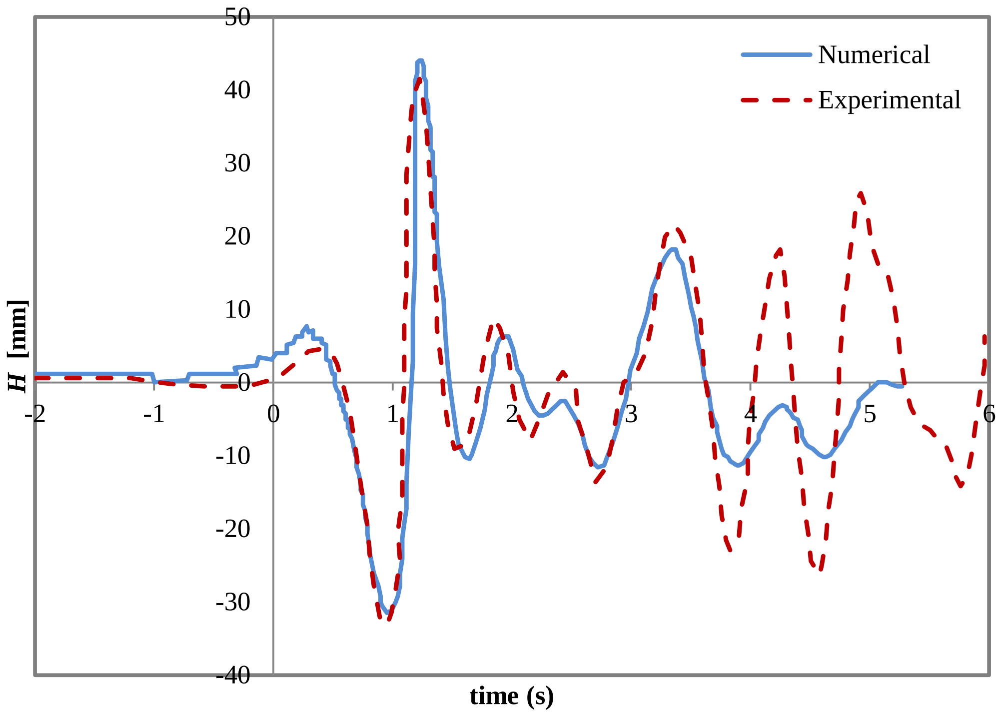

Figure 6.

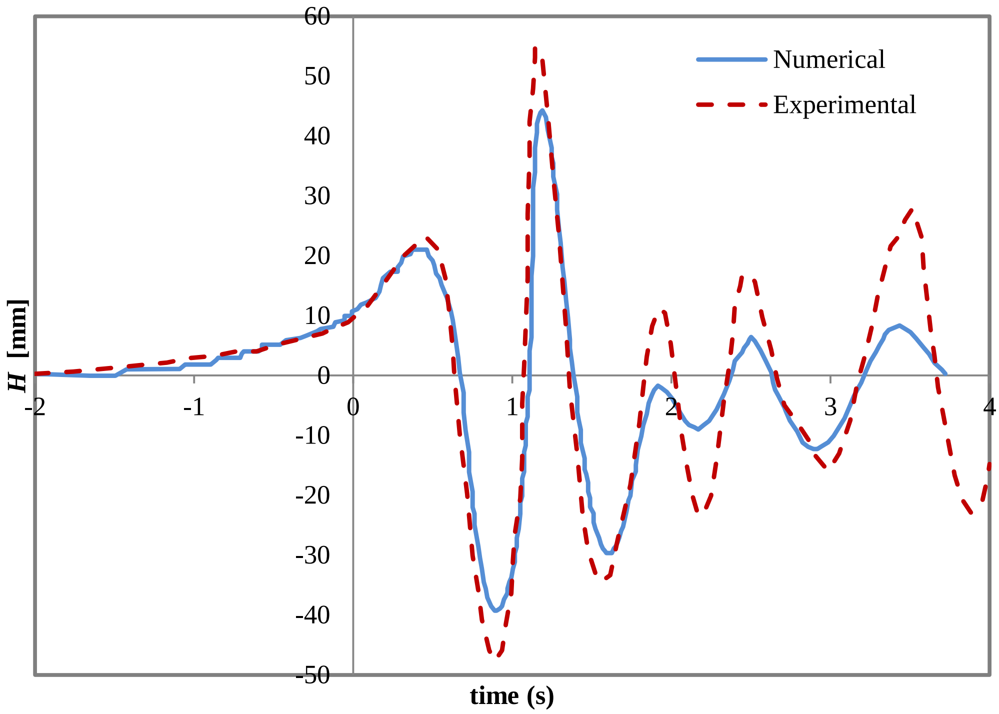

Figure 7.

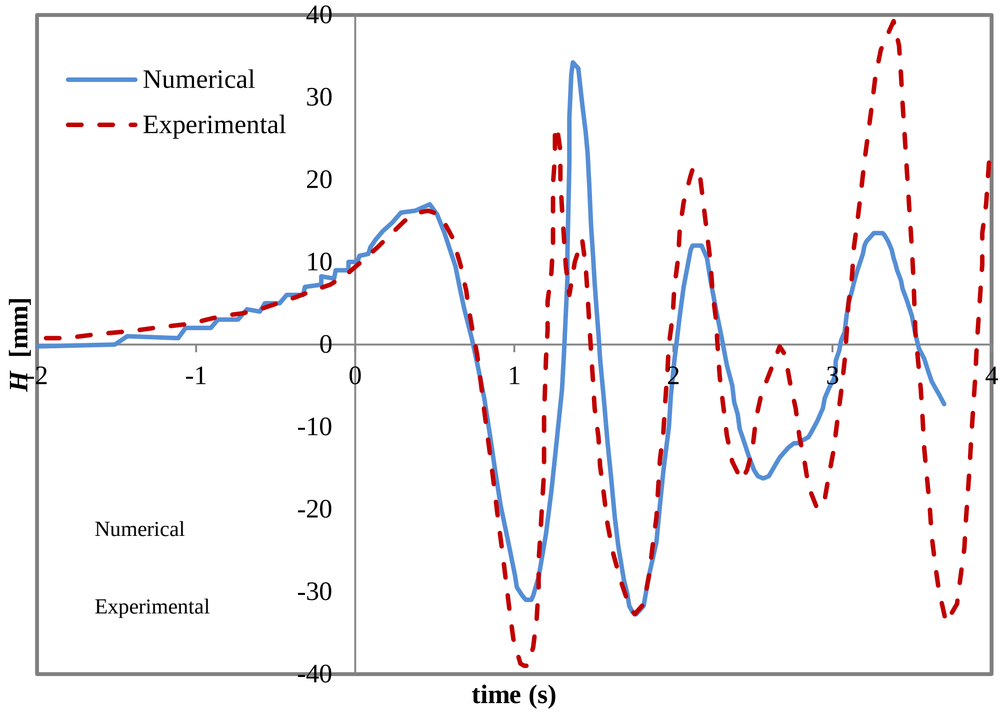

Figure 8.

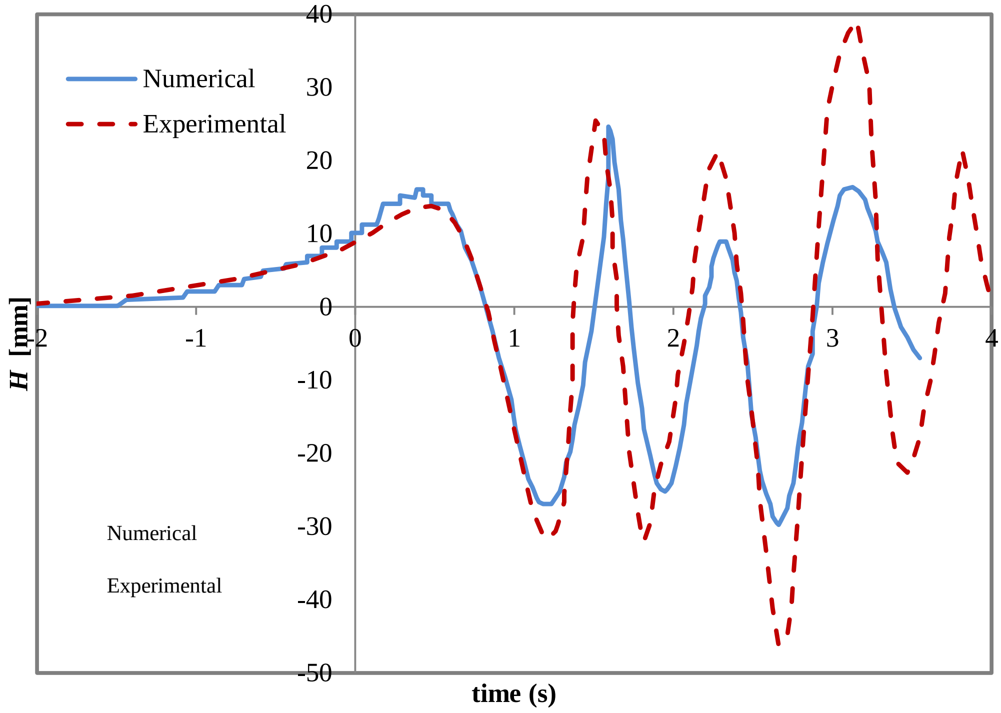

Figure 9.

	Draught (m)	Beam (m)	Angle of attack (deg)	LWL (m)	Displacement (m^3)	Blockage factor
Model 1	0.1	0.3	14	0.40	0.006015	0.0057
Model 2	0.12	0.3	14	0.48	0.00866	0.0068

Table 2.

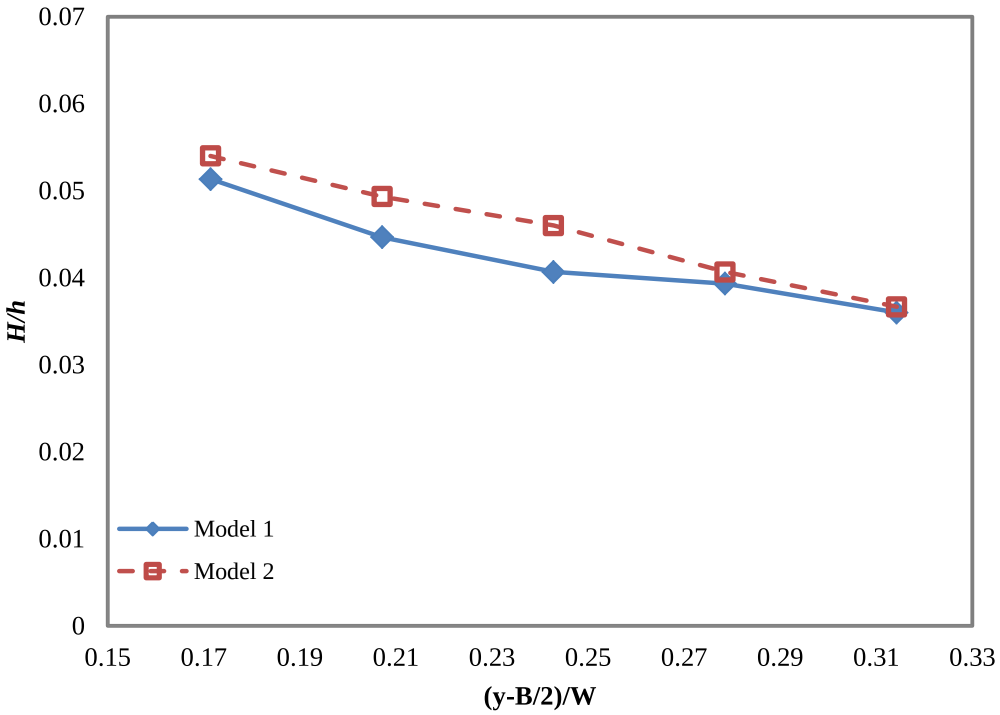

Figure 10.

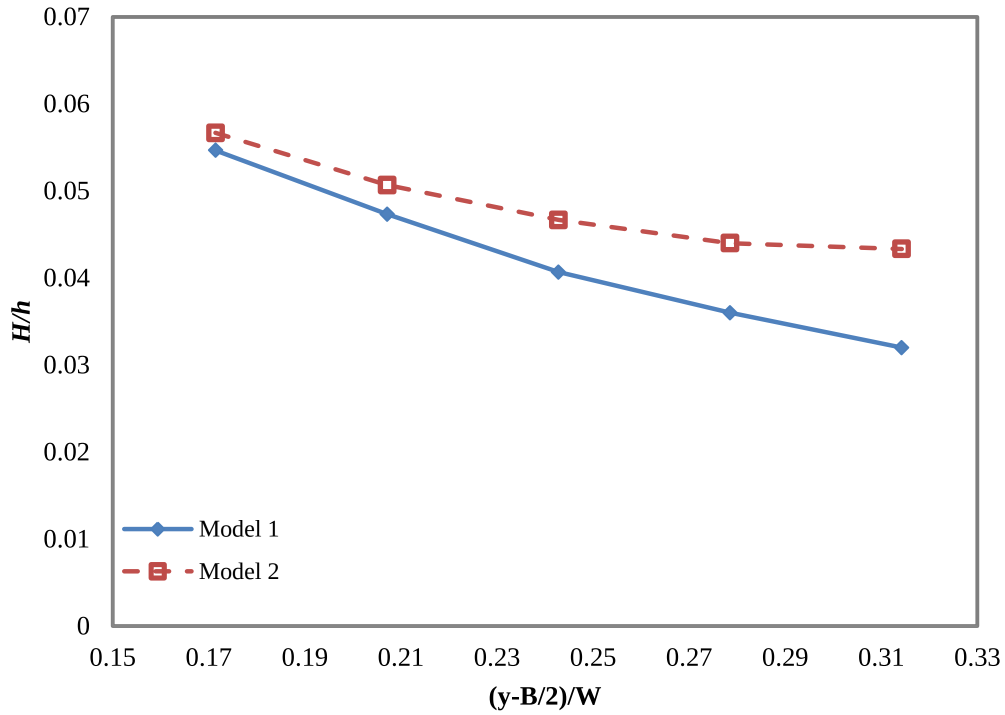

Figure 11.

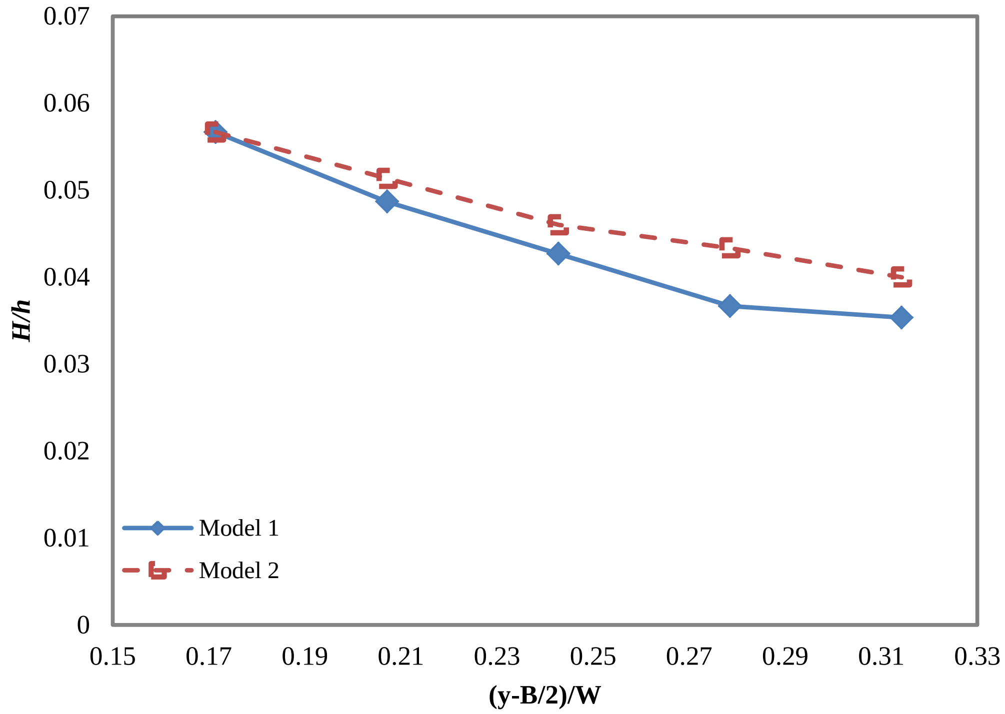

Figure 12.

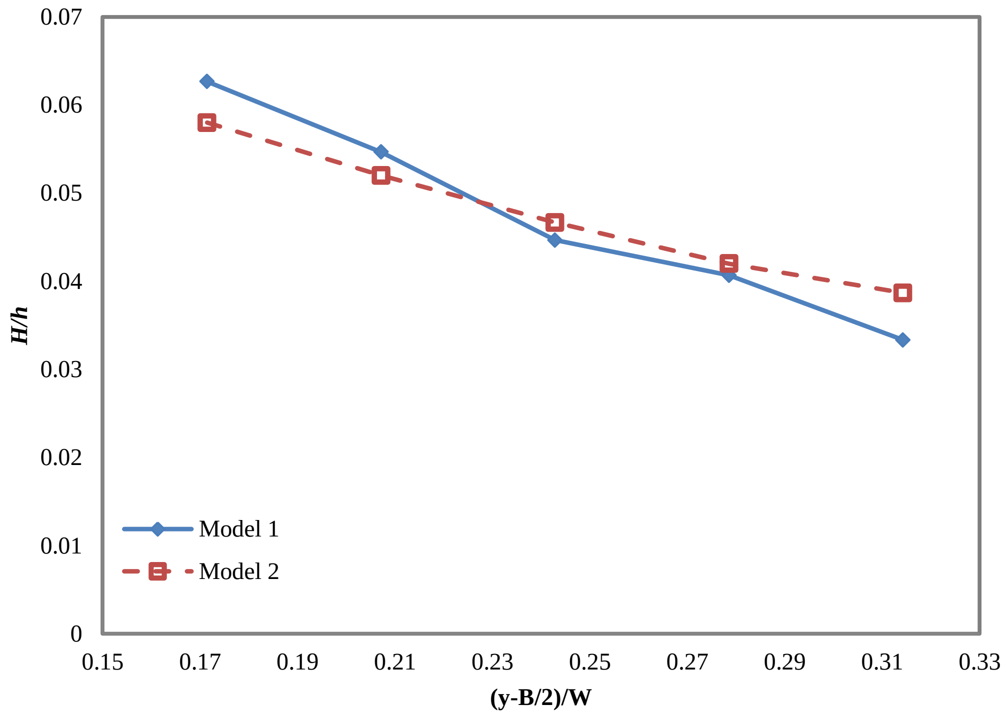

Figure 13.

	Draught (m)	Beam (m)	Angle of attack (deg.)	LWL (m)	Displacement (m^3)	Blockage factor
Model 1	0.1	0.3	14	0.401	0.006015	0.0057
Model 3	0.1	0.3	10	0.567	0.008505	0.0057
Model 4	0.1	0.3	7	0.814	0.01221	0.0057
Model 5	0.1	0.3	4	1.43	0.02145	0.0057

Table 3.

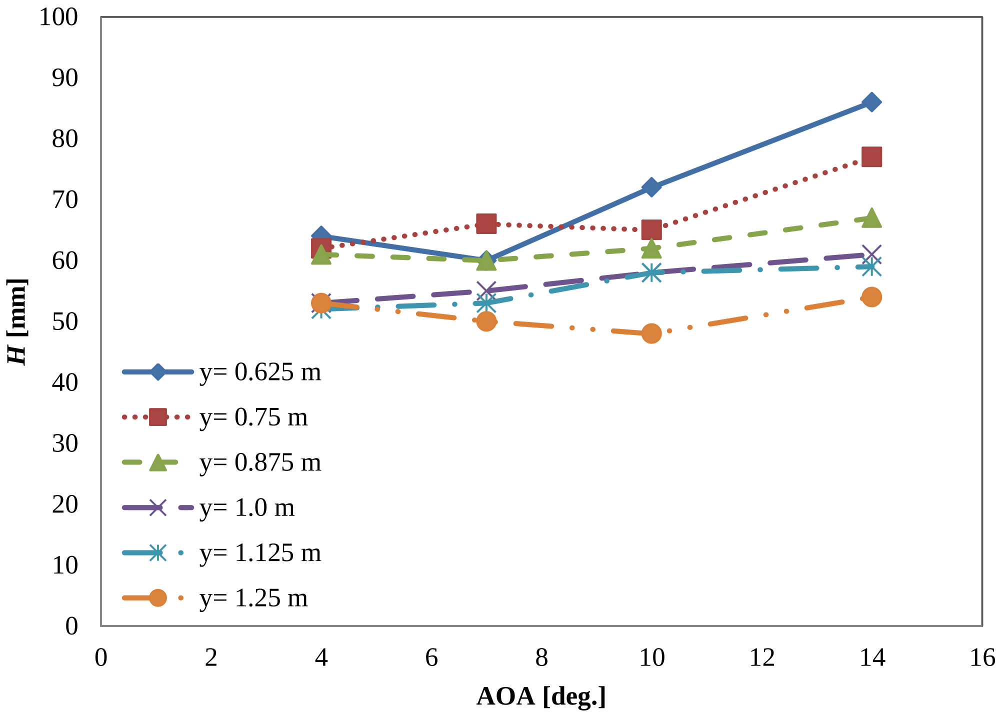

Figure 14.

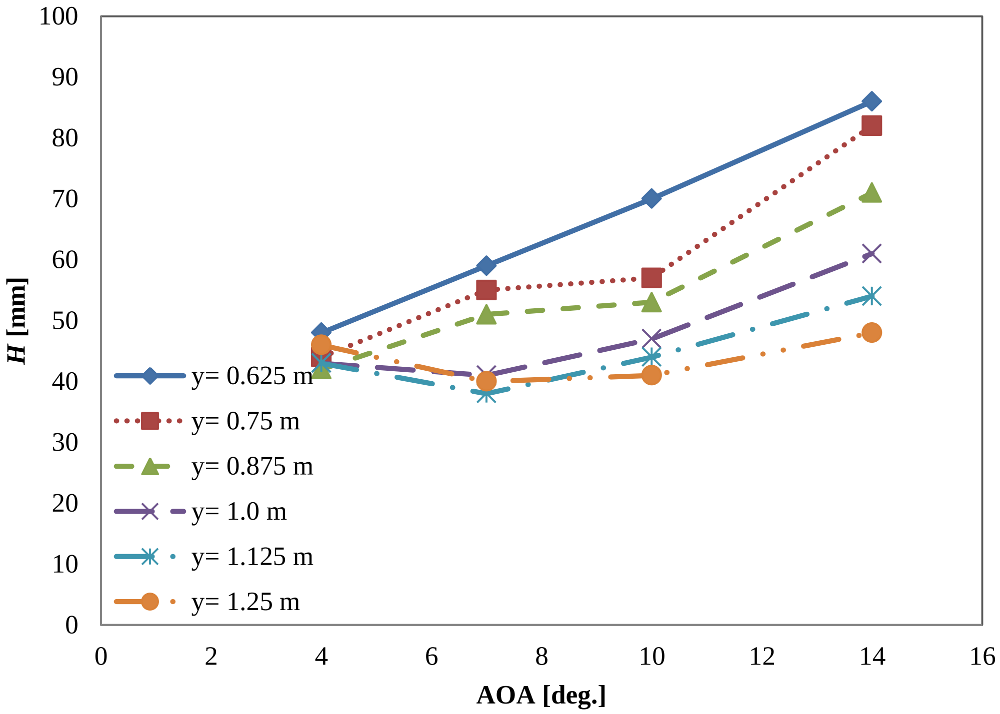

Figure 15.

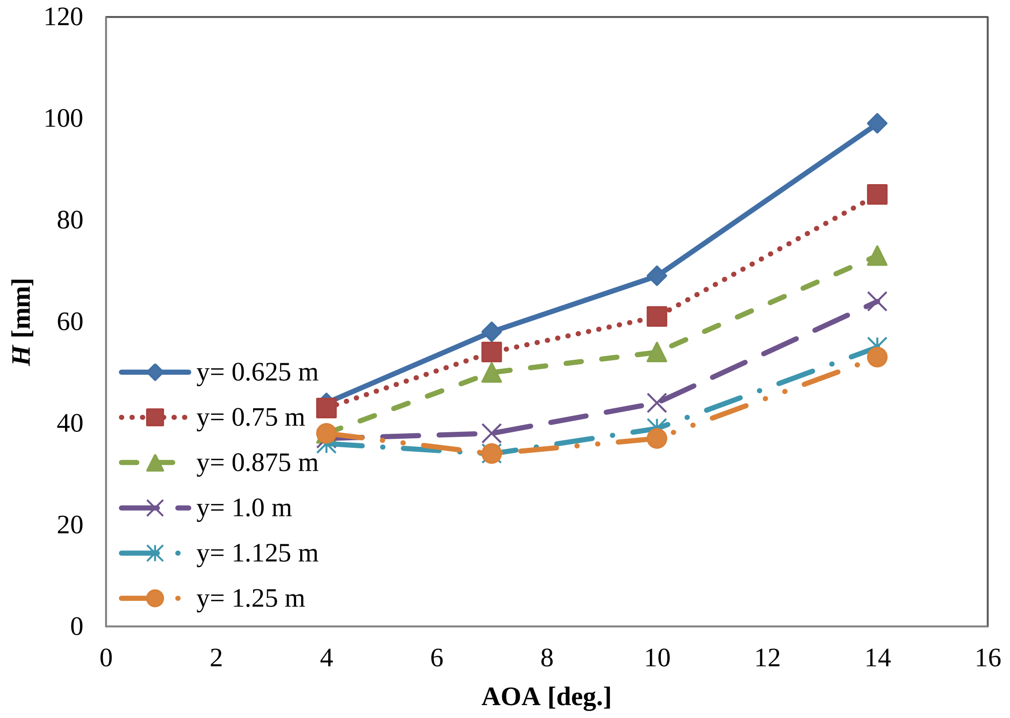

Figure 16.

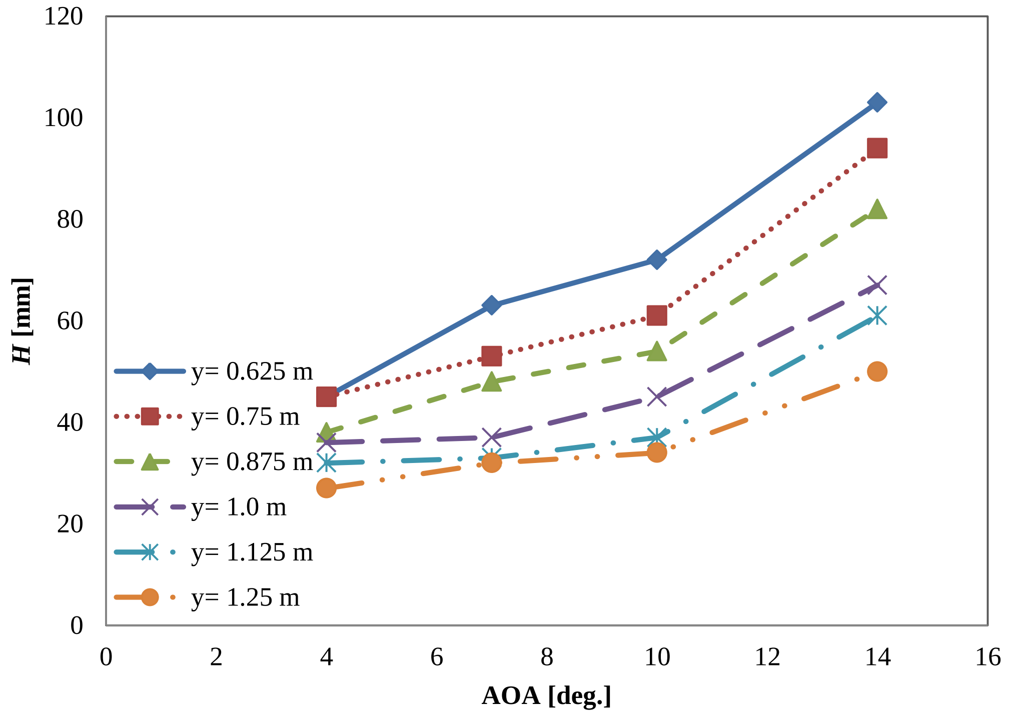

Figure 17.

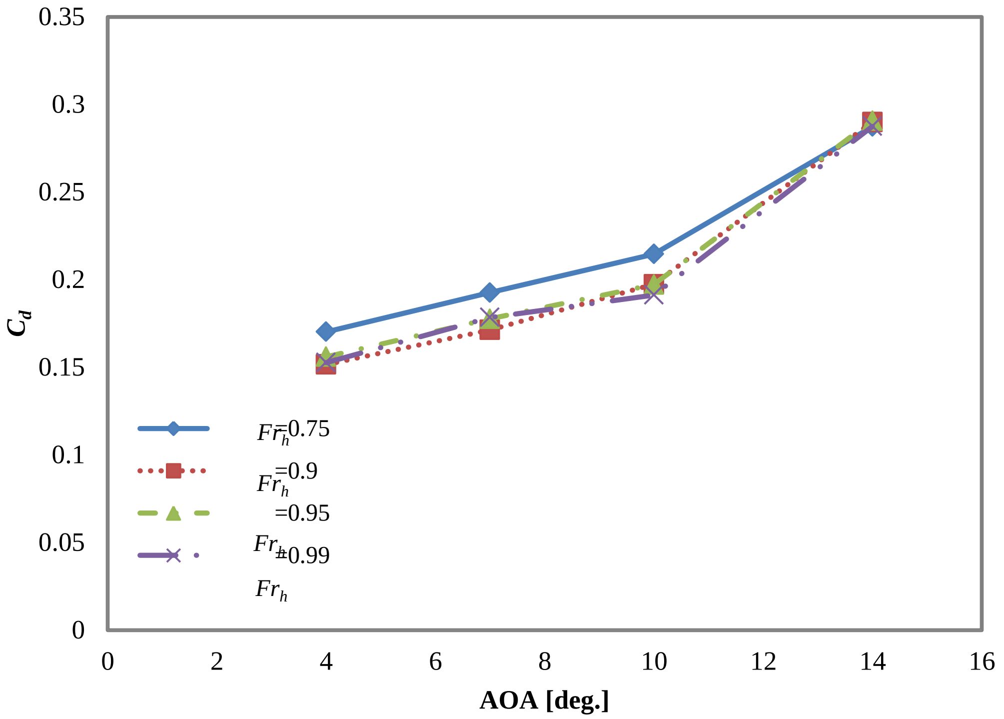

Figure 18.

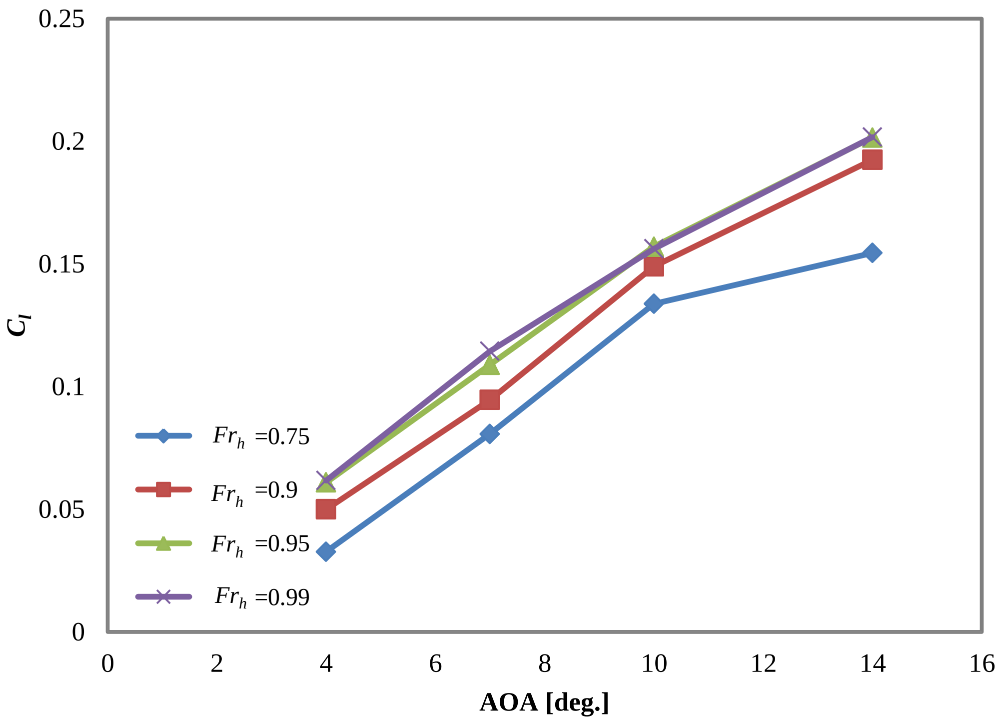

Figure 19.

	Draught	Beam	LWL	Water plane	Angle of attack	Volume displacement

	(m)	(m)	(m)	(m^2)	(degree)	(m^3)
Model 1	0.1	0.3	0.40	0.120	14	0.006
Model 2	0.12	0.3	0.48	0.144	14	0.00866
Model 6	0.1	0.433	0.40	0.174	14	0.00866

Table 4.

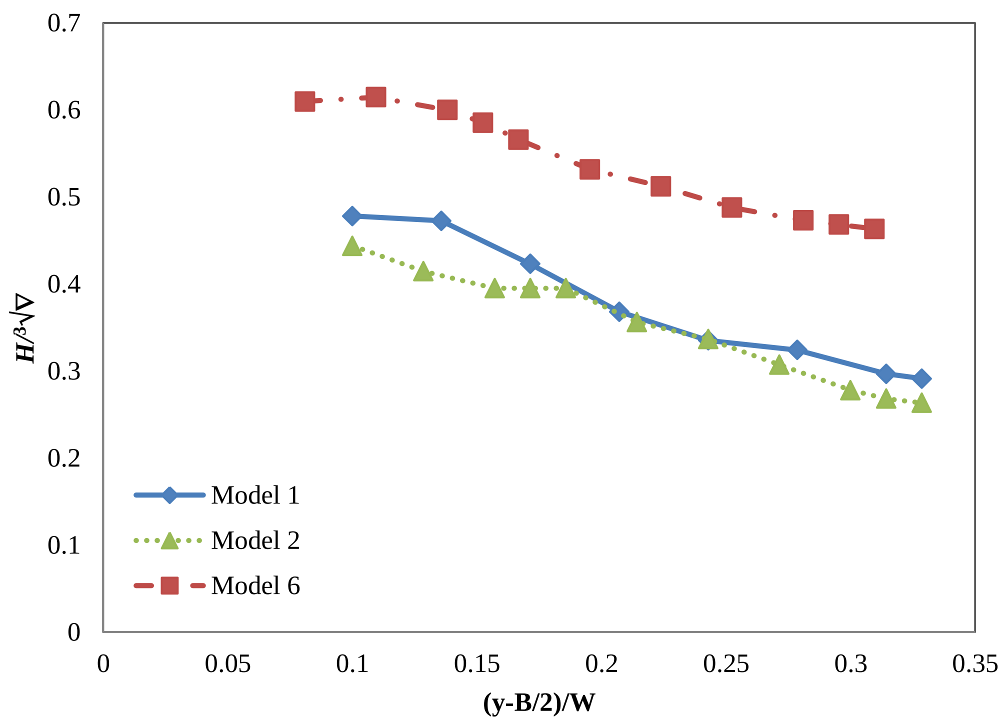

Figure 20.

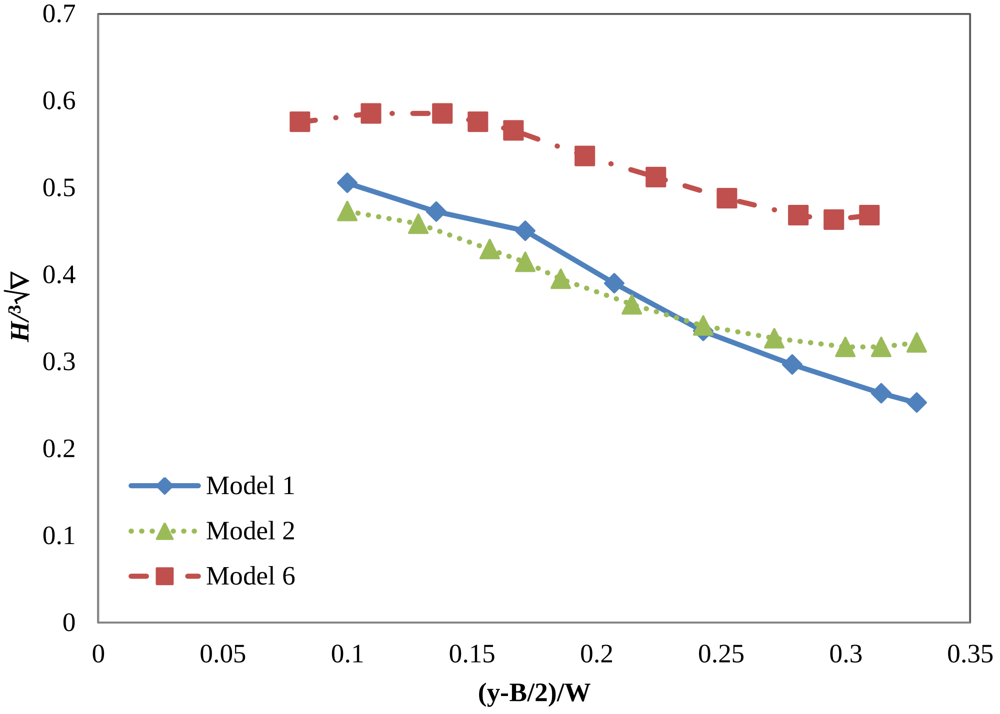

Figure 21.

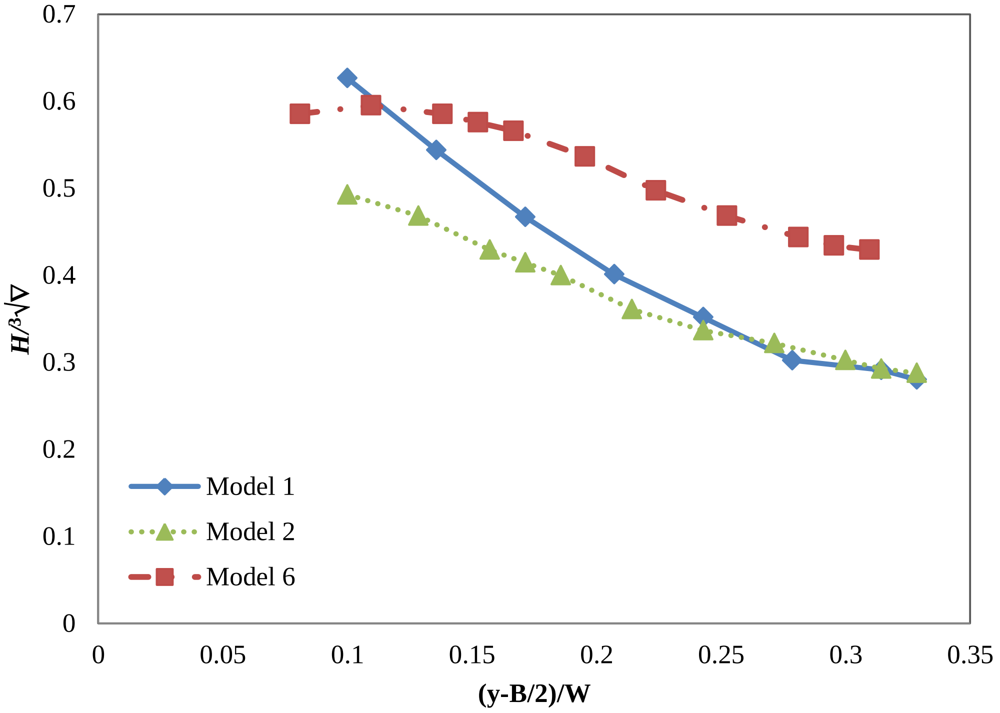

Figure 22.

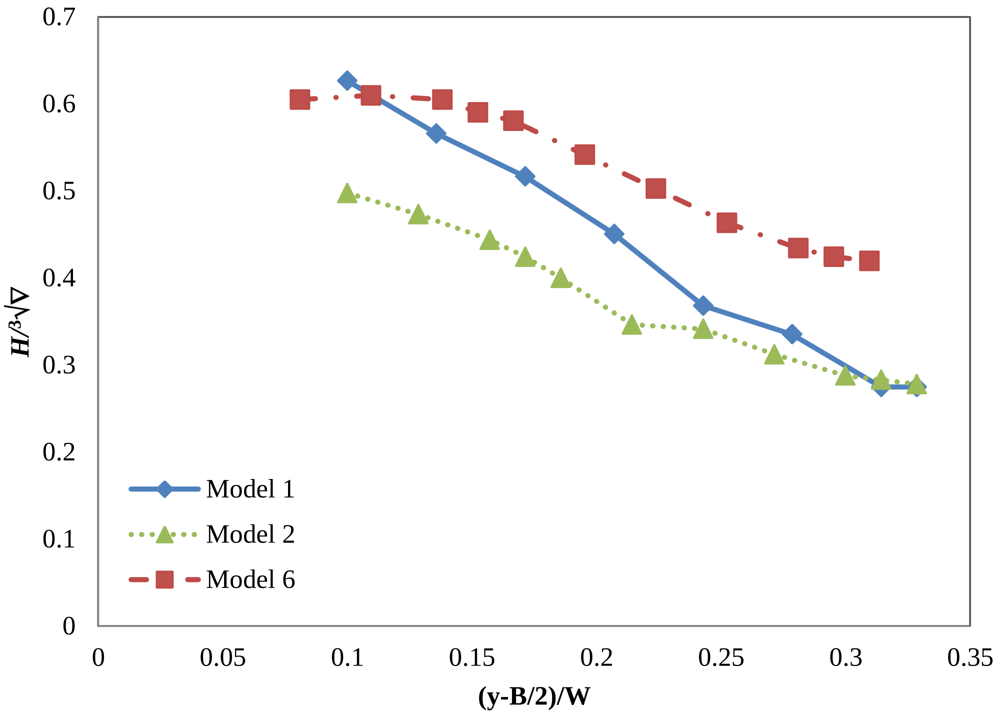

Figure 23.

Beam (m)	0.3
Length of water line (m)	0.4
Angle of attack in front (degree)	14
Angle of attack in stern (degree)	4
Draught (m)	0.1

Table 5.

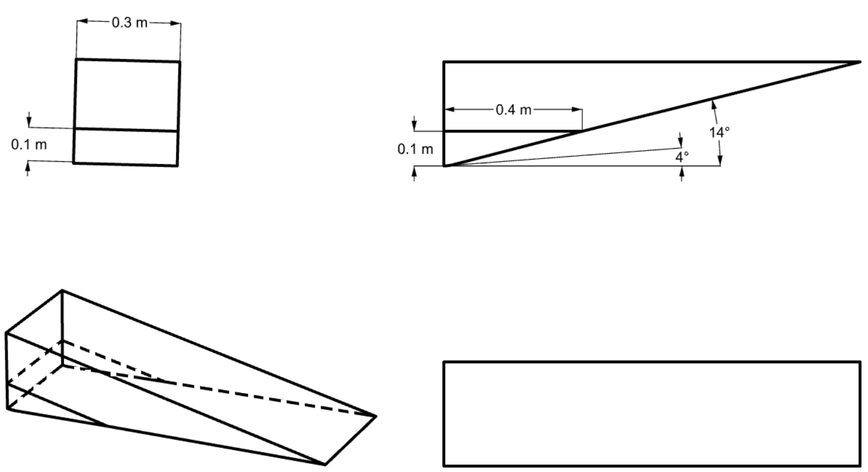

Figure 24.

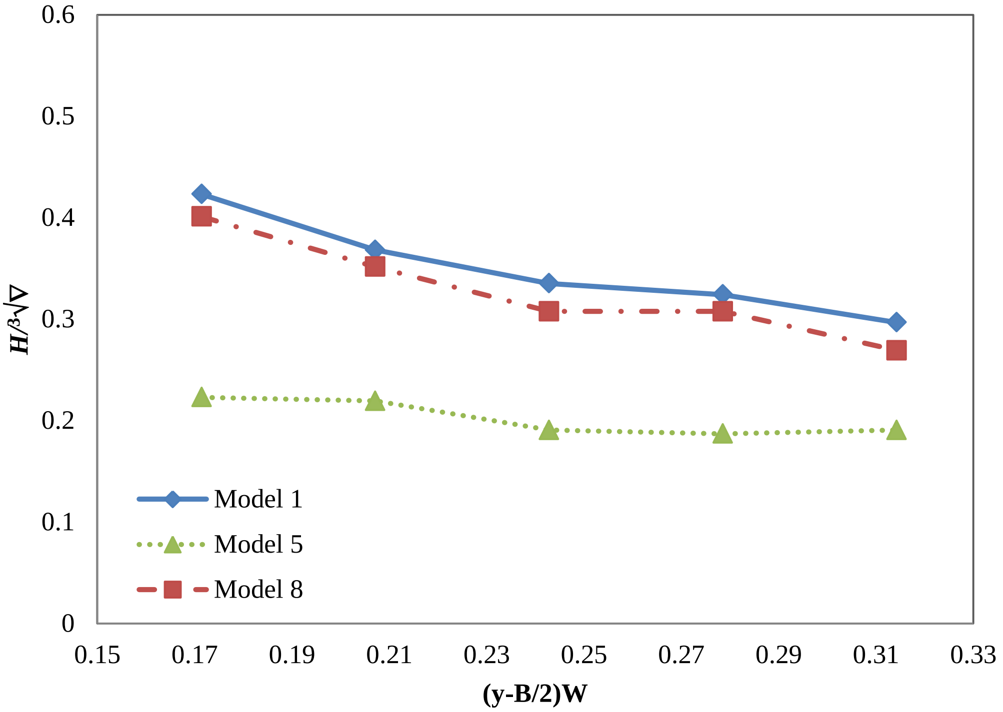

Figure 25.

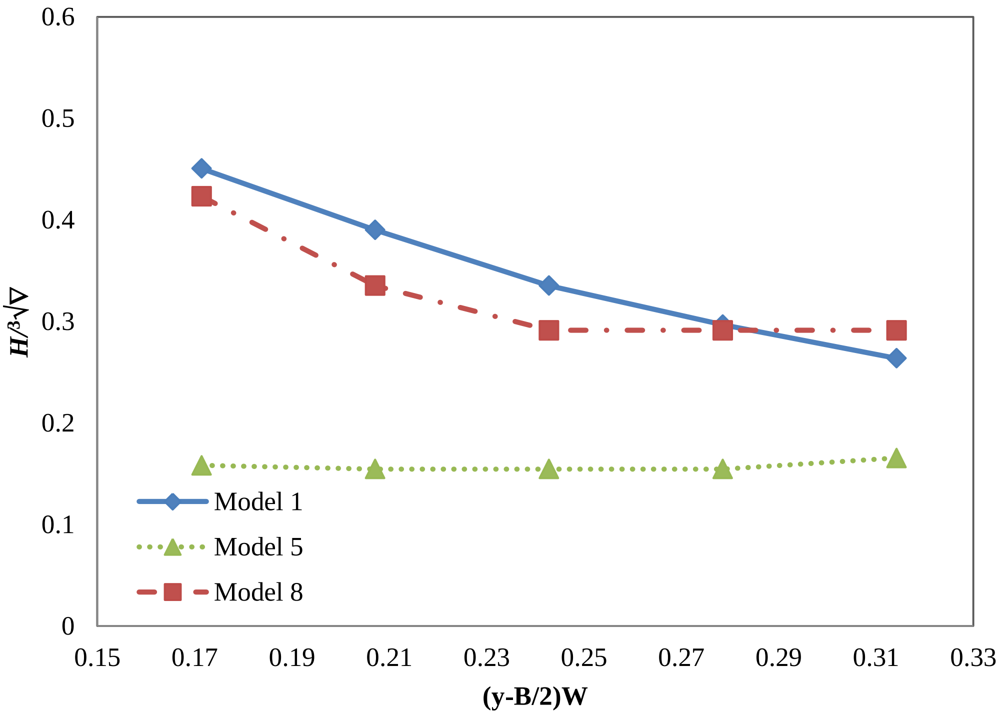

Figure 26.

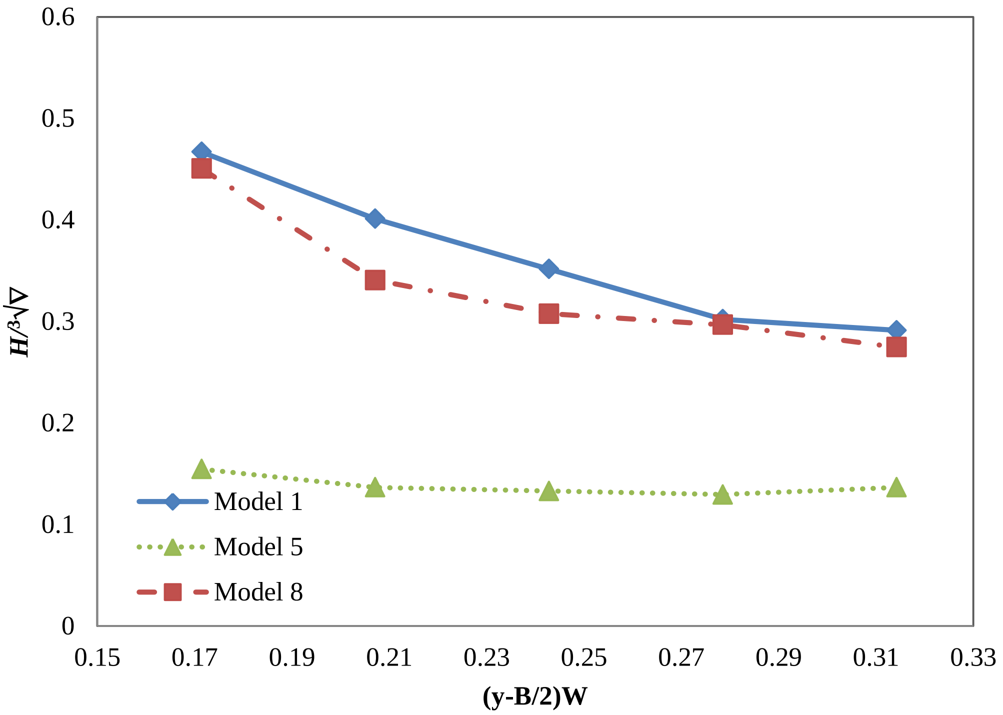

Figure 27.

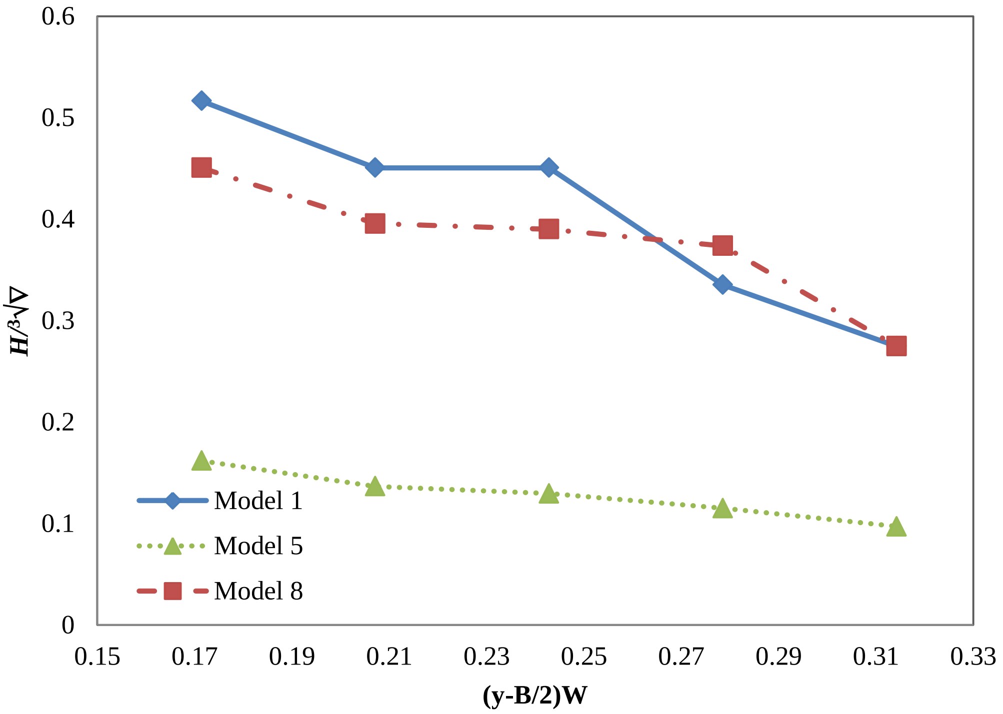

Figure 28.

	h [m] \ V [m/s]	1.66	1.99	2.66
Channel 1	0.4	0.838	1	1.343
Channel 2	0.45	0.79	0.947	1.266
Channel 3	0.5	0.75	0.9	1.2

Table 6.

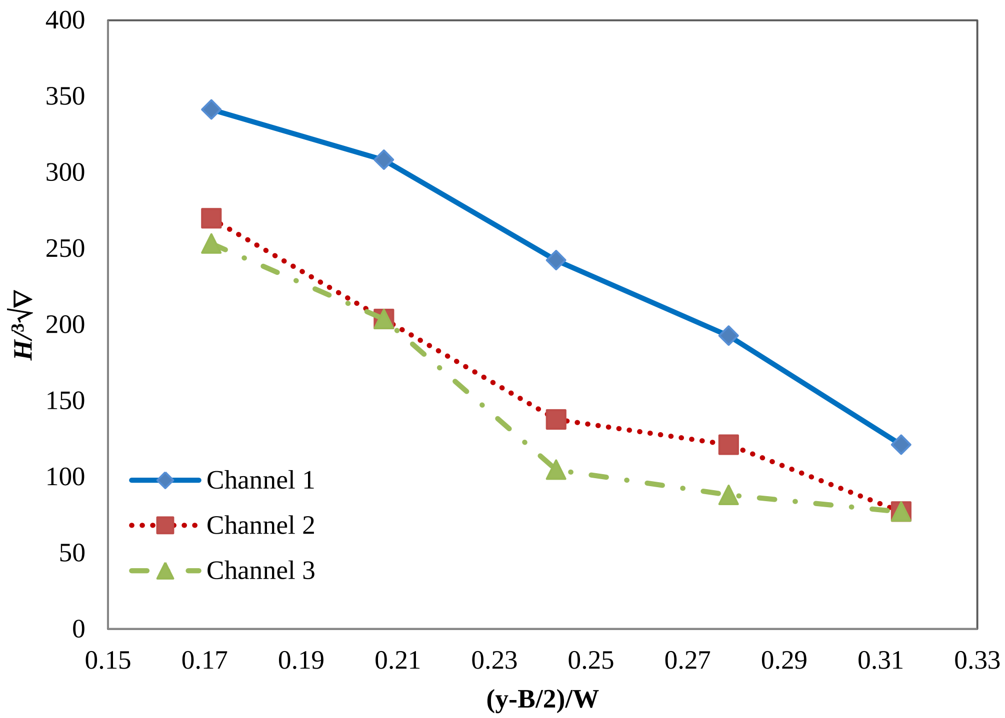

Figure 29.

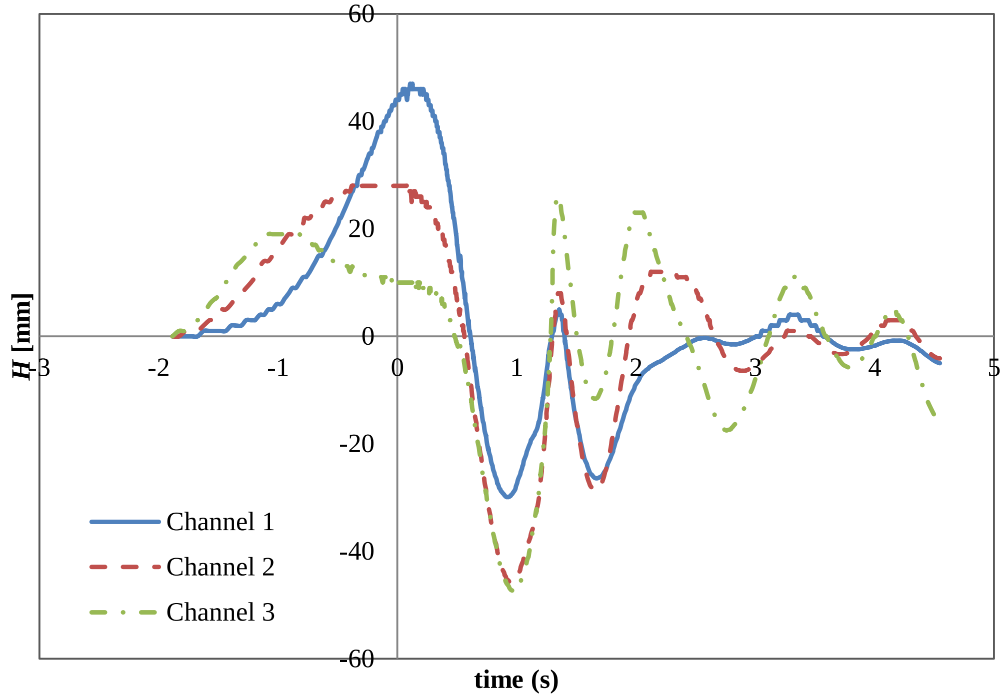

Figure 30.

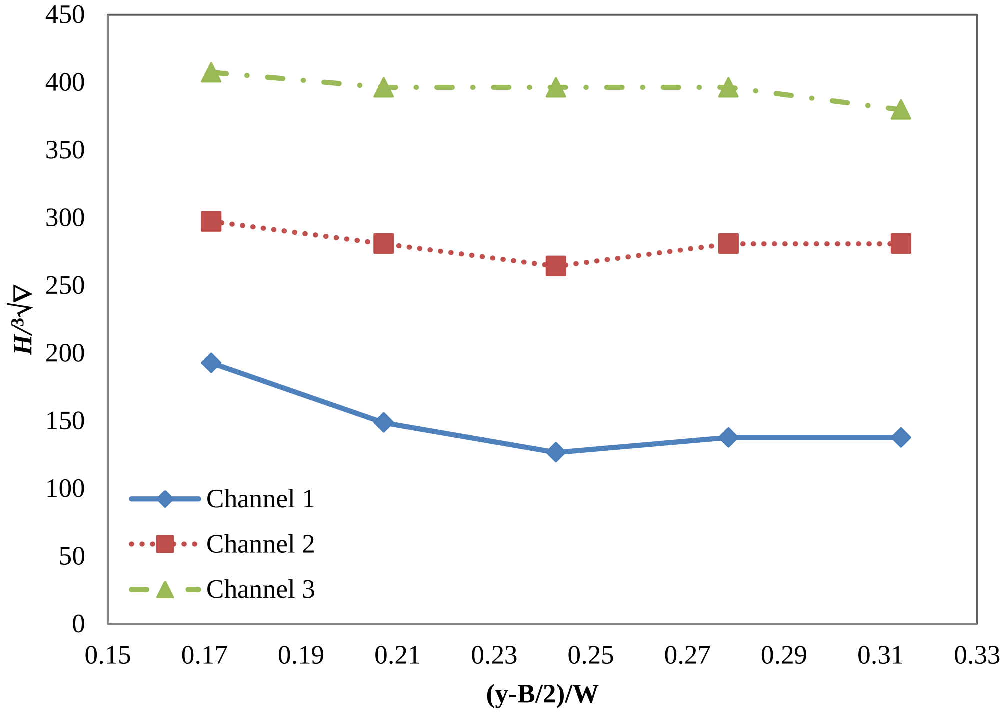

Figure 31.

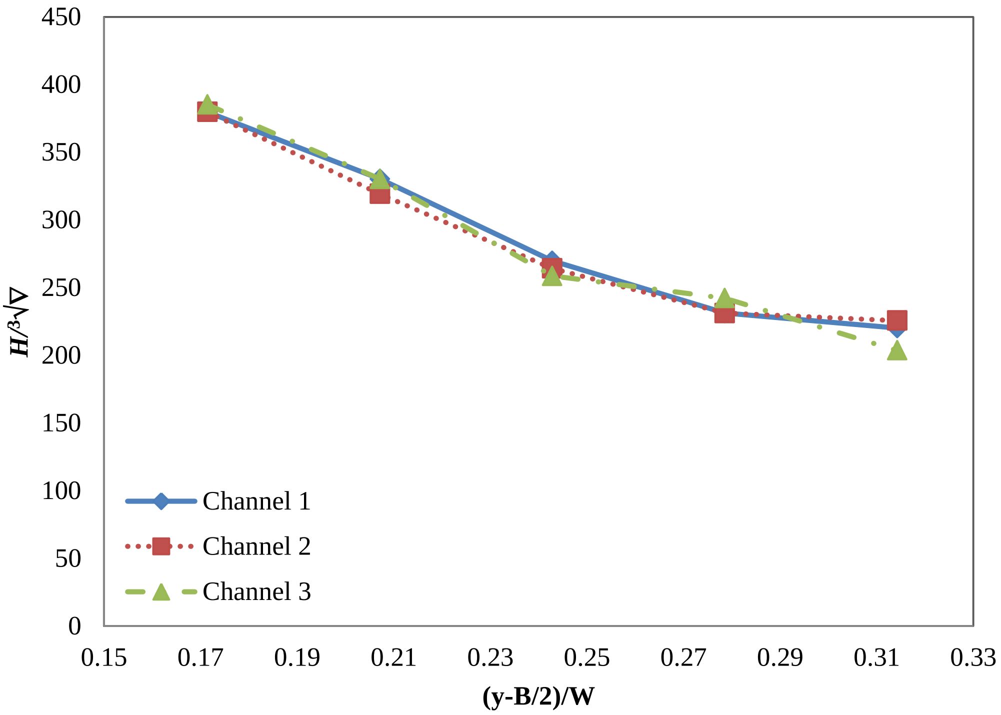

Figure 32.

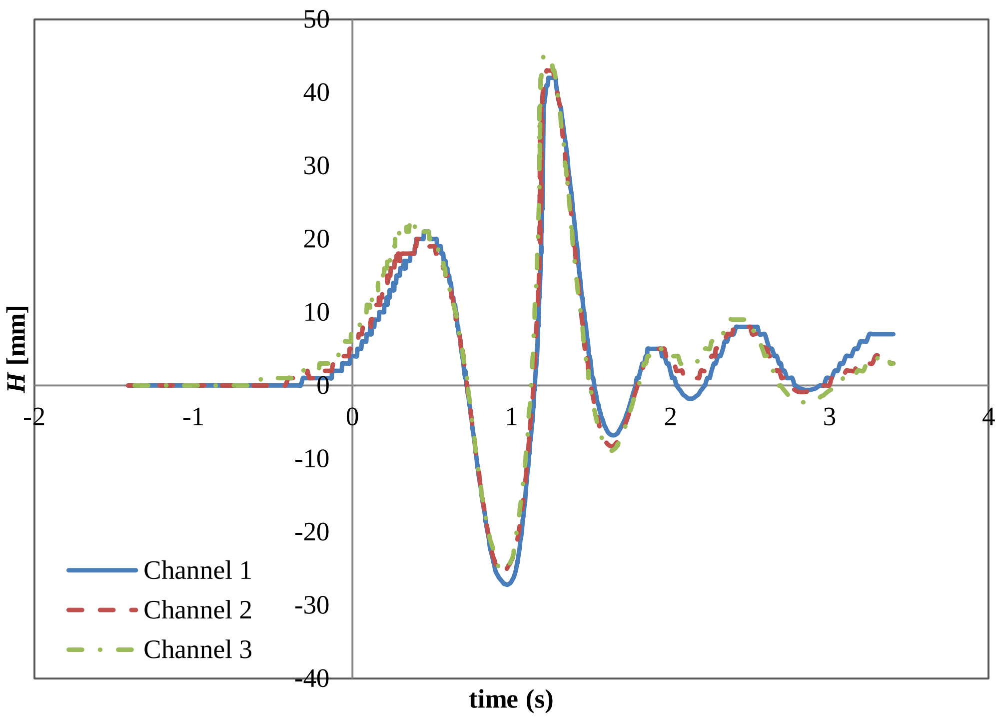

Figure 33.

	Width (m)	Depth (m)	Blockage factor (κ)
Channel 1	3.5	0.4	0.0214
Channel 3	3.5	0.5	0.0171
Channel 4	4.375	0.4	0.0171

Table 7.

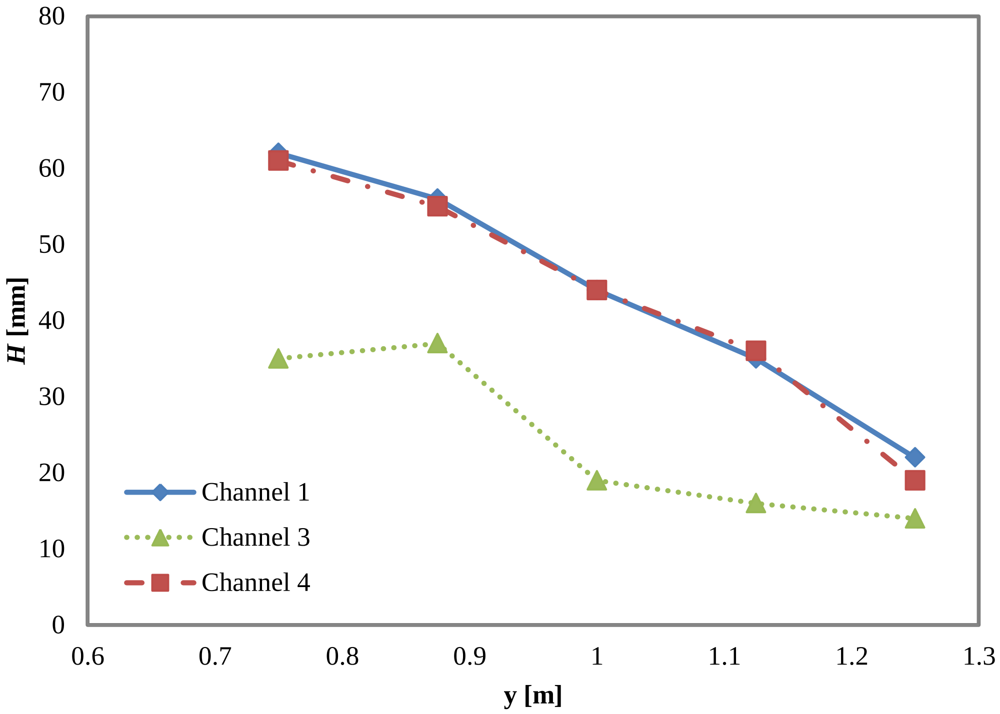

Figure 34.

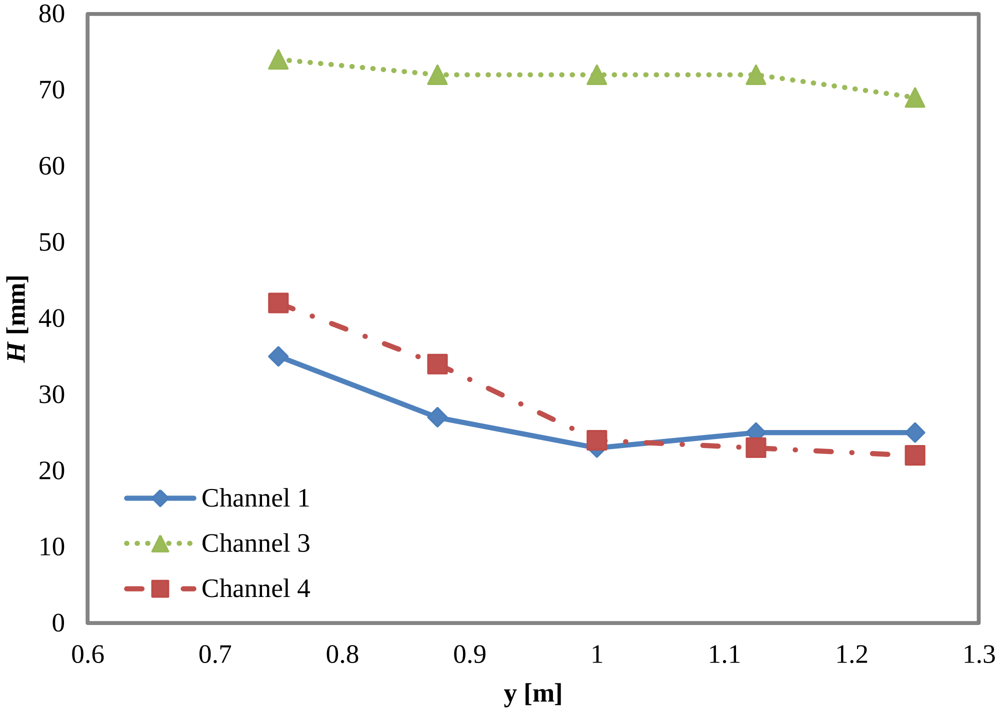

Figure 35.

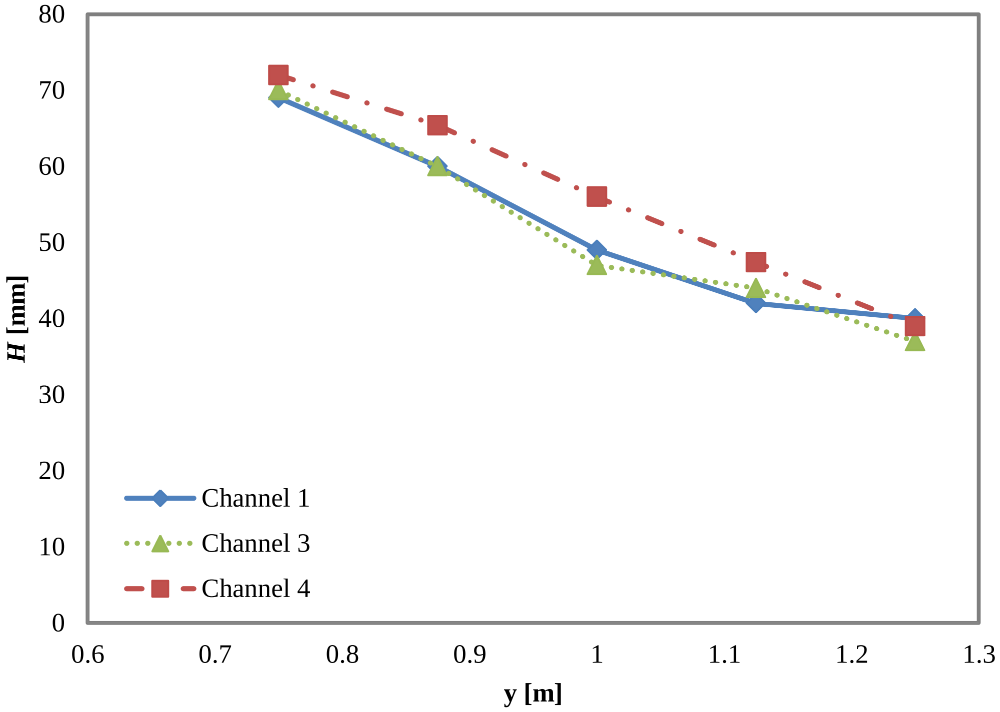

Figure 36.

Appendices

Abbreviations

∇	Volume displacement	H	Wave height
κ	Blockage factor	h	Water depth
χ	Longitudinal distance	LWL	Length of waterline
A_c	Channel cross section area	p	Pressure
AOA	Angle of attack	V	Speed of model
A_s	Model cross section area	W	Width of channel
B	Model beam	WP	Wave probe
C_d	Drag coefficient	y	Lateral distance
C_l	Lift coefficient	y^*	y/W
D	Model draught	ρ	Water density
Fr_h	Depth Froude number		